Tellus (1990), *42A*, 122–139

The structure and evolution of a wintertime occluded front

By PIRKKO SAARIKIVI and TIMO PUHAKKA, *Department of Meteorology, University of Helsinki, Hallituskatu 11-13, SF-00100 Helsinki, Finland*

(Manuscript received 1 December 1988; in final form 16 May 1989)

ABSTRACT

A study, making use of serial radiosonde soundings, weather radar measurements and aircraft reports, has been made of the structure of a deeply occluded wintertime front. The sounding interval during the frontal passage was exceptionally short. The synoptic-scale front-relative flow could be described using the concepts of cyclone warm and cold conveyor belt flows (WCB and CCB) only in its initial stages. During the final stages of the occlusion process, the WCB became diffuse, the CCB weakened and penetrated below the occluded front, and a third relatively dry, cool, and diffluent airflow of mid-tropospheric origin was established above the occluded front. The subsynoptic structure of the occlusion was characterized by a warm frontal zone and, lying above it, a series of "warm tongues" and "cold surges" with a wavelength of about 100 km. The related circulations were also responsible for the formation of the observed banded structures in the snowfall, and agreed with the observed distributions of wind, humidity and temperature. As a whole, the warm tongues and the cold surges together with their related circulations transferred warm moist air upwards and northwards as required in the occlusion process. The observed wavelength, as well as the thermal and kinematic features of the circulations agreed well with the theory of conditional symmetric instability (CSI), though in this case, only small areas with pure CSI were found. The most significant area with CSI was found behind the occluded surface front at the top of the moist layer, while the other areas of CSI, found at higher elevations both above and on the occluded frontal surface were clearly smaller. This was considered to be related to the time history and the life-cycle of the roll circulations probably produced by the CSI.

1. Introduction

The decaying stages of extratropical cyclones were first studied by Bergeron. He discovered in 1919 (Bergeron, 1959) the occlusion process, in which the cold air-mass behind the surface cold front reaches the warm front, resulting in the warmest air in the sector being raised above the surface. Bergeron (1937) also separated the cases of warm and cold occlusions, depending on the temperature difference of the air-masses behind the cold front and ahead of the warm front.

Bergeron's occlusion model was, however, already criticized in the early 1950s. Palmén (1951) argued that "there is no doubt that many 'occluded' cyclones on surface maps have never gone through a real process of occlusion, although they show the same characteristic structure as really occluded polar-front perturbations". Godson (1951) also questioned the occlusion model, and claimed that 95% of occluded cyclones observed on the west coast of North America occur with no surface occluded front but rather an upper cold front and a "trough of warm air aloft".

In their textbook, Wallace and Hobbs (1977) question the very existence of the occlusion process as defined by the classical model. They state that "most occluded fronts are essentially new fronts which form as surface lows separate themselves from the junctions of their respective warm and cold fronts and deepen progressively further back into the cold air". It goes without saying that the concept of a cold front catching up with a warm front and either one overlapping the other, though probably an appropriate scheme close to the point of occlusion, cannot explain all frontal features commonly observed in decaying cyclones.

It was not until the 1960s that observational equipment and techniques had developed to a level at which more detailed experimental studies of occluded fronts became possible. Kreitzberg (1964) observed that the thermodynamical structure of an occlusion was much more complex than was assumed in the simple Norwegian model. He found many subsynoptic "hyperbaroclinic" zones in connection with the main synoptic scale frontal zone. In a case study of a warm occlusion (Kreitzberg, 1968; Kreitzberg and Brown, 1970), pre-frontal surges (pulses of cold air) and "tongues" of warm air above the warm frontal zone were observed. The air above the warm, moist tongues was often potentially unstable, resulting in convective "generating cells" above the warm front.

Recent experimental studies of occlusions reveal a complex nature similar to that already observed by Kreitzberg. Matkovskii and Shakina (1982) and Ragette (1984) have studied the structure of warm occlusions and Hobbs et al. (1975), Houze et al. (1976) and Herzegh and Hobbs (1981) cold occlusions.

In spite of recent observations, there are still many fundamental questions to be answered. For example, we do not yet know for sure which are the basic dynamical processes producing the strongly baroclinic mesoscale zones within the broader frontal zones and why the precipitation is organized into mesoscale bands, even though some plausible theories on their origin exist. These questions can be answered definitively only by studying the thermodynamical structure of occlusions in very great detail.

This paper presents a case study of a wintertime deeply occluded cyclone. In addition to a synoptic-scale conveyor belt analysis, a more detailed smaller-scale analysis will be presented based mainly on serial radiosoundings. The role of the structures found in redistributing heat will be discussed, as well as the possible instability mechanisms generating those features. Factors related to the decay of the frontal structures will also be briefly approached.

2. Observational setup

The observations for the present case study were carried out during MERASEX-83, the Mesoscale Rain and Snowfall Experiment at the Department of Meteorology, University of Helsinki. A detailed description of the observational system and procedures is given in Saarikivi and Puhakka (1986).

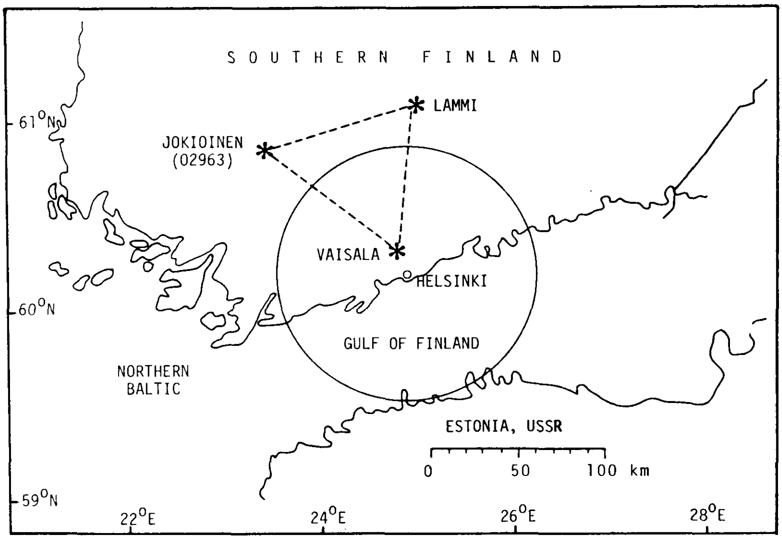

Fig. 1. Map of the measurement area. Sounding stations are depicted by asterisks. The range of measurement of the radar is also shown.

The observations presented in this paper rely mainly on data from serial soundings and the X-band weather radar of the University of Helsinki. A map showing the locations of the sounding stations and the measuring radius of the radar is shown in Fig. 1. The radar was used to digitally record the three-dimensional structure of echoes at 10 min intervals. From these data, time–height sections of the average radar reflectivity inside our measuring area were derived. Series of instantaneous low-elevation PPI-pictures were also used.

The sounding system of the MERASEX-83 experiment consisted of 3 radiosonde sounding stations. The distances between stations were approximately equal and a little less than 100 km. Each station was equipped with a similar automatic sounding system. New light-weight sondes were used, in which temperature and humidity were measured with capacitive rapid-response sensors. Wind profiles were derived using what is known as the Omega Navaid wind-finding system based on the world-wide navigational network. As a result, wind profiles with an almost constant accuracy independent of the elevation angle were obtained together with very detailed temperature and humidity data.

Before and after the frontal precipitation area, the sounding interval was 3 h, while during the active phase of the system passage, soundings were made at 1-h intervals. Special emphasis was laid on the simultaneity of the soundings at each station. Each sounding reached well above the tropopause. Vertical resolution was approximately 60 m, corresponding to the 10 s sampling interval.

For further analysis, the data were projected onto an evenly-spaced grid, using where necessary simple linear interpolation both in the vertical and in time. Basic and derived parameters were analysed at intervals of 100 m in the vertical. The 1-h time interval between soundings corresponds in this case to a horizontal resolution in the vicinity of the main frontal surface of about 30 km. Thus, the basic data were able to represent phenomena having wavelengths of more than about 200 m in the vertical and 60 km in the horizontal. With the derived parameters (divergence, vorticity, vertical velocity, growth rate of CSI) based on data from the sounding triangle, horizontal wavelengths representable by the data were about 100 km due to the additional smoothing.

3. Synoptic-scale analysis

The observations were carried out on 3–4 January 1983, when a deeply occluded warm occlusion passed Finland approximately from west to east. The related cyclone was tracked for 4 days earlier from the coastal areas of Newfoundland. Infrared METEOSAT satellite pictures in Fig. 2 show that by 3 January, the cyclone over Scandinavia was already deeply occluded (Fig. 2a) and that the front (denoted by A) was rapidly weakening due to the diffluent flow over northern Europe.

On 4 January, at 0700 GMT (Fig. 2b), the occluded front in which we are interested is just over Finland and its banded cloud structure is clearly visible, especially in the enlargement of Fig. 2b over Scandinavia (Fig. 2c). The next member of the cyclone family (denoted by B) is seen over southern Scandinavia with the typical lambda-shaped cloud deck of a mature cyclone.

Fig. 3 presents a time series of the evolution of the cyclone for the two consecutive days before its arrival in Finland. Surface frontal analyses are presented together with the conveyor belt flows (CBF), a concept originally adopted by Harrold (1973) and Browning et al. (1973). In the analyses, the warm conveyor belt flow (WCB) and the cold conveyor belt flow (CCB) correspond to the main airflows relative to the warm front, and later, relative to the warm occluded front. The CBFs were analysed using relative winds on constant moist isentropic surfaces. As data for the main pressure levels (850, 700 and 500 hPa) were only available for restricted areas, the isentropic relative streamlines could not be analysed in detail based on this data only. The conceptual models for WCB and CCB by Harrold (1973) and Carlson (1980) were applied where it was felt feasible, naturally in harmony with the real observations including also satellite pictures. The values of the moist potential temperature θ_w were 9–12°C and 0–4°C for WCB and CCB, respectively.

It should be noted that originally, the CBFs

Fig. 2. METEOSAT infrared channel pictures over Europe (a) 3 January 1983 at ca. 1500 GMT, (b) 4 January 1983 0700 GMT, (c) as in (b) but enlarged over Scandinavia. The coldest (highest) cloud tops appear as the lightest (yellow) shades.

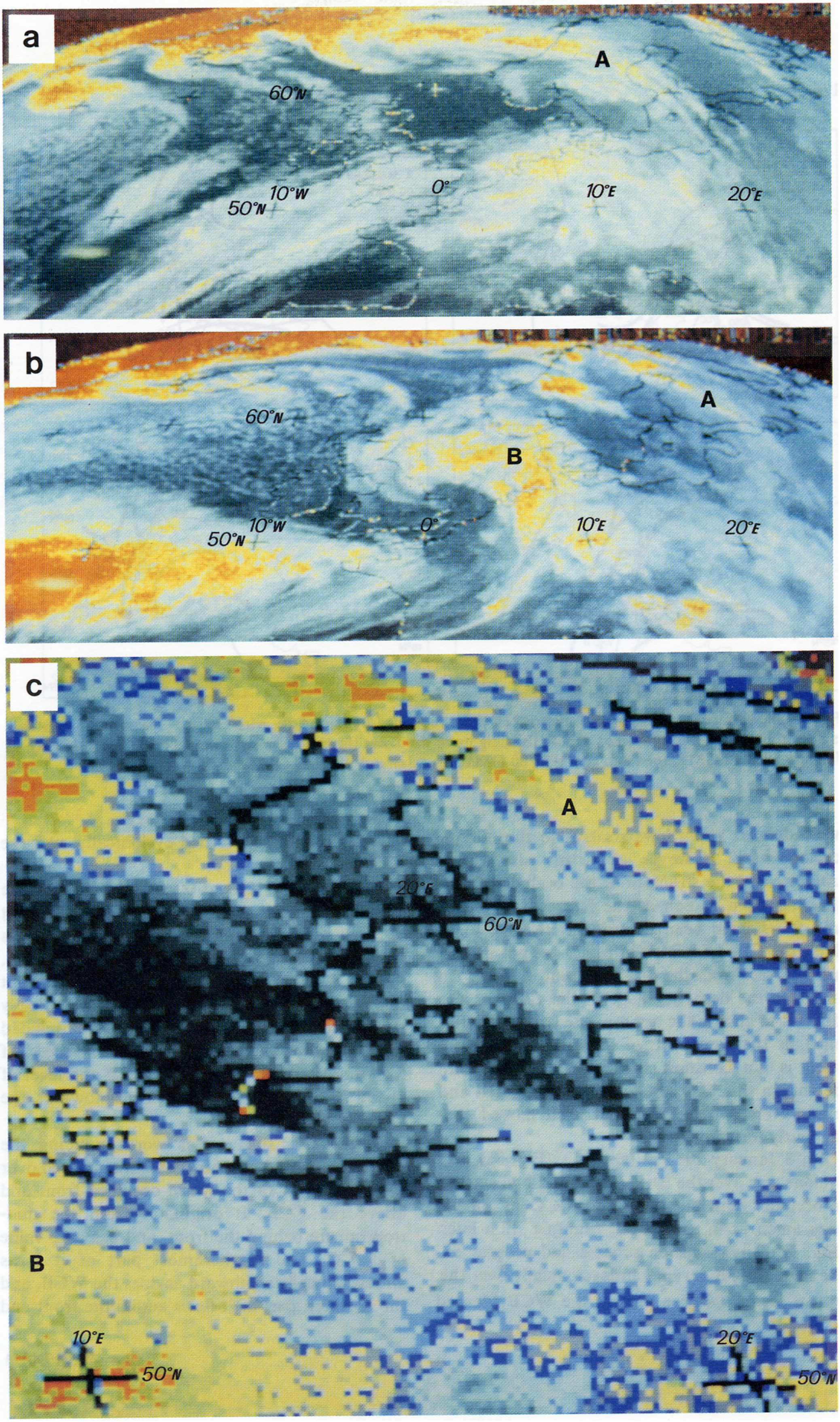
a
A
60°N
10°W
50°N
0°
10°E
20°E
b
60°N
A
B
10°W
50°N
0°
10°E
20°E
c
A
20°E
60°N
B
10°E
50°N
20°E
50°N

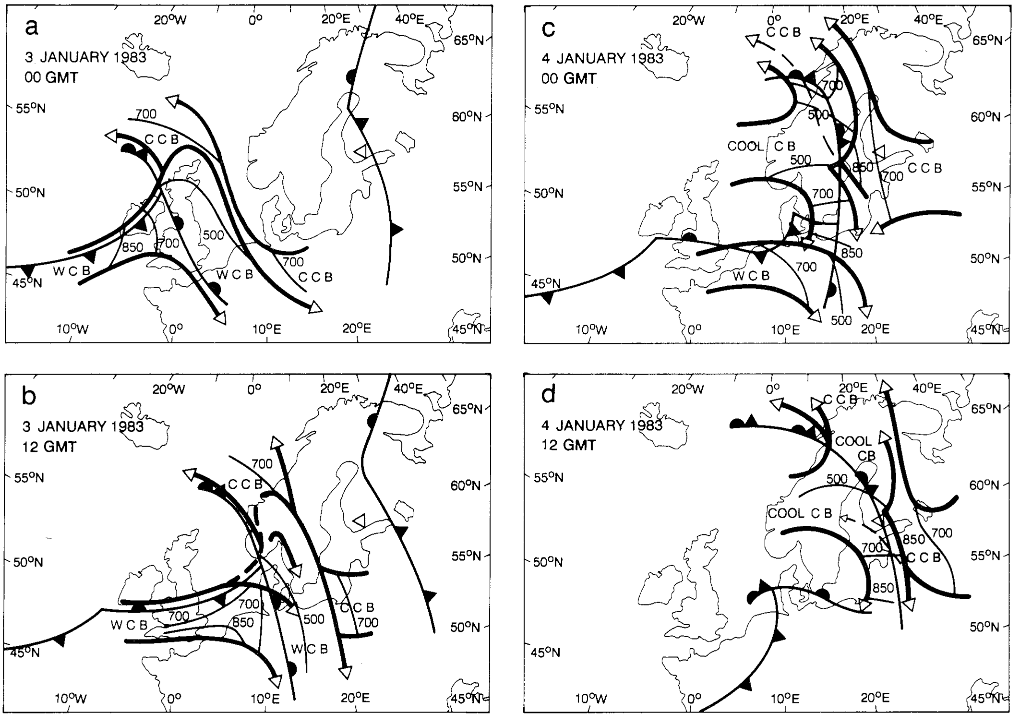

Fig. 3. The surface fronts and the conveyor belt flows (bounded by thick lines with arrows). The sounding triangle is also indicated. Thin solid lines denote the heights of the flows (in hPa), for (a) 3 January 1983 00 GMT, (b) 3 January 1983 12 GMT, (c) 4 January 1983 00 GMT, (d) 4 January 1983 12 GMT.

were defined as airflows relative to the moving cyclone itself. However, as in this case we are interested in the structure of the occluded front, that has been chosen as the frame of reference and flows have been determined relative to it. Thus the CBFs depicted in Fig. 3 are not necessarily correct from the original point of view. All in all, in the decaying stage of the cyclone, it is difficult to choose the appropriate frame of reference, as the movement of the depression centre itself is not constant and also may vary with height. In this case, the cyclone decelerated and even reversed while the front itself moved continuously forward.

On 3 January 1983 at 00 GMT (Fig. 3a), the cyclone was over the British Isles and had started to occlude. Both the WCB and the CCB appear very much as in a textbook example. 12 h later (Fig. 3b), the occlusion process had progressed, the major WCB curving anticyclonically over the warm sector, while a part of the WCB (dashed line in Fig. 3b) still turned cyclonically over the occluded front.

On 4 January 1983 at 00 GMT (Fig. 3c), the occluded front was situated over the eastern coast of Sweden and the centre of the depression was far away over the Norwegian sea. At this time, the WCB can no longer be easily recognized, but it is clear that the WCB does not turn cyclonically northwards. The CCB flows towards the occluded front ahead of the point of occlusion. Ahead of the front, it is clearly discernible at the level of about 700 mb and flows northwest towards the low-pressure centre.

During this stage, it is worth noticing the relatively dry and cool air that is transported over the moist layer of the warm occluded front and above the CCB. It originates from the mid-troposphere behind the front, and has a θ_w value of 5–7 °C. The southernmost part of it turns anticyclonically southward as does the WCB, and the northern part of it flows across the front and turns northward. The height of the cool flow above the surface front at the point where it breaks into two branches is about 4 km, and from there the flow descends both to north and to south.

Thus in addition to the main WCB and CCB couple located typically with respect to the cold and warm fronts, there seems to be a diffluent "cool CBF" behind the occluded front. The diffluent low-θ_w flow maintains suitable conditions for potential instability in frontal areas close to the cyclone centre but no longer in the middle parts of the occluded front or near the occlusion point. This structure may be an indication of the process by which the frontal system loses its connection with the mother-cyclone. Looking at the satellite pictures (Fig. 2), one can see that high clouds exist only in the northern parts of the occluded front but not near the supposed location of the occlusion point and the WCB.

In Fig. 3d on 4 January 1983 at 12 GMT, the occluded front had moved further east, the point of occlusion had progressed further south, and some remains of the WCB, the CCB and the "cool" CBF can perhaps still be recognized.

Amongst the few conveyor belt analyses from deeply occluded cyclones to be found in the literature, one may mention that of Kurz (1988). However, the analyses in Figs. 3c, d show that this occlusion seems to be different from that presented by Kurz. In his case, part of the original WCB turned cyclonically and flowed along the occluded front towards the low pressure centre. In our case, it is clear that the original WCB air was not flowing into the region of the occluded front. Air which was flowing over the warm occluded front originated at higher levels within the mid-tropospheric "cool" air-mass behind the occluded front, and at lower levels from the CCB, mainly within the planetary boundary layer.

4. Mesoscale analysis of the occlusion

4.1. Single station time-height sections

The time-height sections derived from the radiosoundings reveal the complex thermodynamic nature of the occluded frontal system. In each of the following cross-sections, the vertical extent is 10 km. The 24-h time-scale corresponds roughly to a 700 km horizontal distance across the occluded front. The ill-defined surface front passed over our sounding triangle, which was located slightly to the south of the most diffluent area of the cool CBF, at approximately 12 GMT.

The time-height sections from the 3 sounding stations were very similar to each other. The same features which were observed almost simultaneously at Vaisala and Lammi (see Fig. 1) were observed somewhat earlier at Jokioinen. The sounding station Lammi is used in the following examples, because it had the best uninterrupted series of soundings.

Fig. 4a represents the time-height section of temperature. The baroclinic zones deduced from the temperature field are superimposed. There were 2 main warm frontal layers on top of each other. In addition to these, 2 secondary warm frontal structures may be observed: one between the main frontal layers and another above.

The upper warm frontal zone is related to the second cyclone (B in Fig. 2) approaching our occluded front from the southwest. Between these 2 major frontal layers, a 3rd weaker one may be observed, which is related to the top of the moist air-mass in the first cyclone and is caused by the interaction of the large-scale subsidence from above and the frontal ascending motion below.

In the lowest warm frontal zone, at least 2 tongues of warm air (denoted by W1 and W2 in the figures), using the notation of Kreitzberg (1964), and possibly another 2 weaker ones can be seen. Between the warm frontal layers, a series of surges of cold air with weak cold-frontal-like patterns were observed. The most prominent of these are denoted by C1–C4 in the figures. These can be seen in Fig. 4b as zones of steeper wet-bulb potential temperature gradient slanting from upper left to lower right, approximately perpendicular to the main warm frontal zones. These correspond to the "leafed" nature of occluded fronts and the "hyper-baroclinic zones" observed by Kreitzberg (1964). The most prominent cold surges and tongues of warm air can also be observed from the cross-sections of wind and humidity, which are shown in the following.

Fig. 4c shows the time-height section of relative humidity. A layer about 3 km deep behind and above the lower warm frontal zone was at or near saturation. High humidity values near the tropopause at 5 GMT are very likely observation errors due to icing. Beneath the lowest warm frontal zone, the air was extremely dry: values of relative humidity as low as 8% were observed. This is a typical feature ahead of and beneath warm frontal zones and was already observed by Vuorela (1953) from routine synoptic soundings. Just ahead of the surface front, a moist cool density current type flow was observed. It was evidently due to precipitation falling from above and evaporating into the dry air-mass below, thus cooling the air ahead of the surface front. The lowest part of the warm occluded front itself was very diffuse and could not be identified from surface wind observations, but the leading edge of the density current was easily recognizable at the ground.

The most interesting features in the humidity cross-section were, however, the high and low humidity couplets situated on top of the moist frontal layer and at least one also within the moist layer. Their similarity with the rearward sloping cloud canopies with dry tongues of air behind them as observed by Browning et al. (1973) is striking, and it may be well justified to assume that in this study and in that by Browning et al., the observed features are manifestations of similar dynamic processes occurring in both cases. The cold surges observed from the temperature distribution coincide with the moisture patterns, so that the air ahead of the cold surge is more humid than behind it.

Fig. 4d represents the u-component of the wind, which in this case is also very close to the cross-frontal wind. The speeds of the 2 main warm frontal zones coincide very closely to the u-component of the wind at the frontal surface. The speed of the upper front (14 m/s) was almost twice that of the lower (8 m/s), so that the 2 frontal zones continuously approached each other and overlapped. This speed difference must be kept in mind when interpreting the time–height sections as spatial cross-sections. The pattern of the cross-frontal wind corresponds to the observations by Browning and Harrold (1969) of a warm frontal zone. The layer of the strongest vertical shear is well aligned with the lowest warm frontal zone.

Fig. 4e shows the v-component of the wind, which in this case is almost front-parallel. A southerly low-level wind maximum of 14 m/s can be seen just below the lowest part of the warm frontal zone. The structure, the position and also the flow speed of the low-level jet again correspond well with the observations by Browning and Harrold (1969). Reflections of the cold surges can also be observed in the front-parallel wind field: there is a tendency for a stronger southerly flow ahead and a weaker southerly or even a northerly flow behind the cold surges. These differences in the v-component are more pronounced with the most baroclinic cold surges C2 and C3, while with surges C1 and C4 such differences in the v-component cannot be found. Because of the systematically larger v-component within the warmer air in front of the cold surges in comparison with that behind them, the net effect is the transport of heat towards the north.

4.2. Divergence, vorticity and vertical velocity

Estimates for the horizontal derivatives needed in calculating the horizontal divergence and the vertical component of the relative vorticity were obtained using simultaneous measurements from the three sounding stations. The horizontal drifting of balloons during ascent was taken into account when estimating the divergence. In the Omega wind-finding system used in the experiment, the repeatability figure is of the order of 0.5 m/s and is constant with height. The standard deviation of wind component error is of the order of 1 m/s (Nash and Schmidlin, 1987). Thus, in a sounding triangle of the size used here, the divergence can be estimated with an accuracy of the order of 10^{-5} s^{-1}, provided that the measured values of wind represent mean values on the sides of the triangle. As values of divergence in the mesoscale and especially in frontal regions easily exceed this limit by an order of magnitude, the evaluation of divergence and also of the vertical velocity based on the divergence were considered feasible, even though the sub-grid scale effects cause an additional error to the results.

Vertical velocities were estimated from the anelastic form of the continuity equation by integrating it in 100 m vertical steps from the surface up to a height of 10 km. Raw values of w so obtained were further adjusted to fulfil the mass balance requirement between the surface and 10 km where w was assumed to be zero. At the lowest level, w was calculated taking into

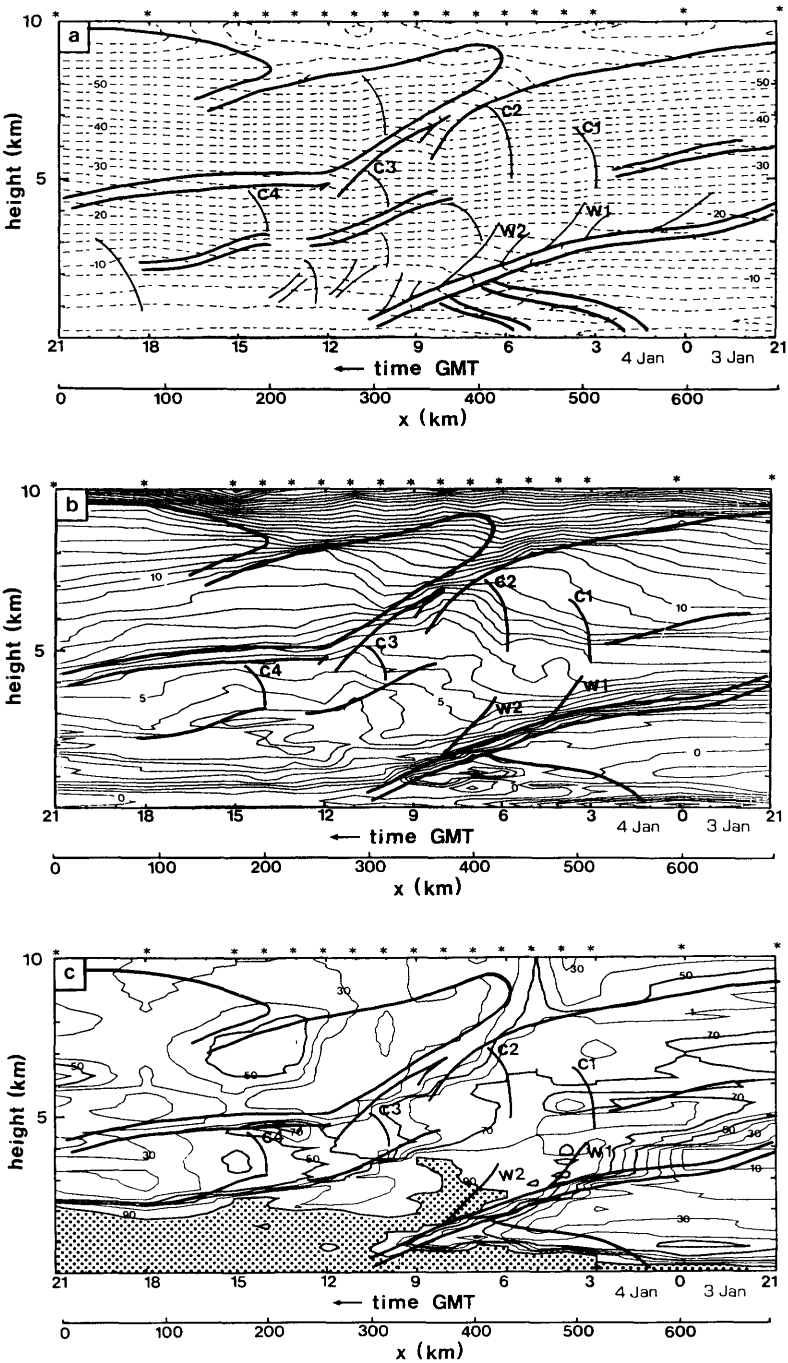

Fig. 4. Time–height sections on 3–4 January 1983 at the Lammi sounding station. Asterisks at the top of each figure indicate times of radiosonde soundings. The horizontal scale is obtained assuming a constant west–east system propagation velocity of 8 m/s. (a) Temperature (°C). Baroclinic zones are indicated with heavy full lines. The most prominent cold surges and warm tongues are denoted by symbols C1–C4 and W1–W2, respectively. (b)

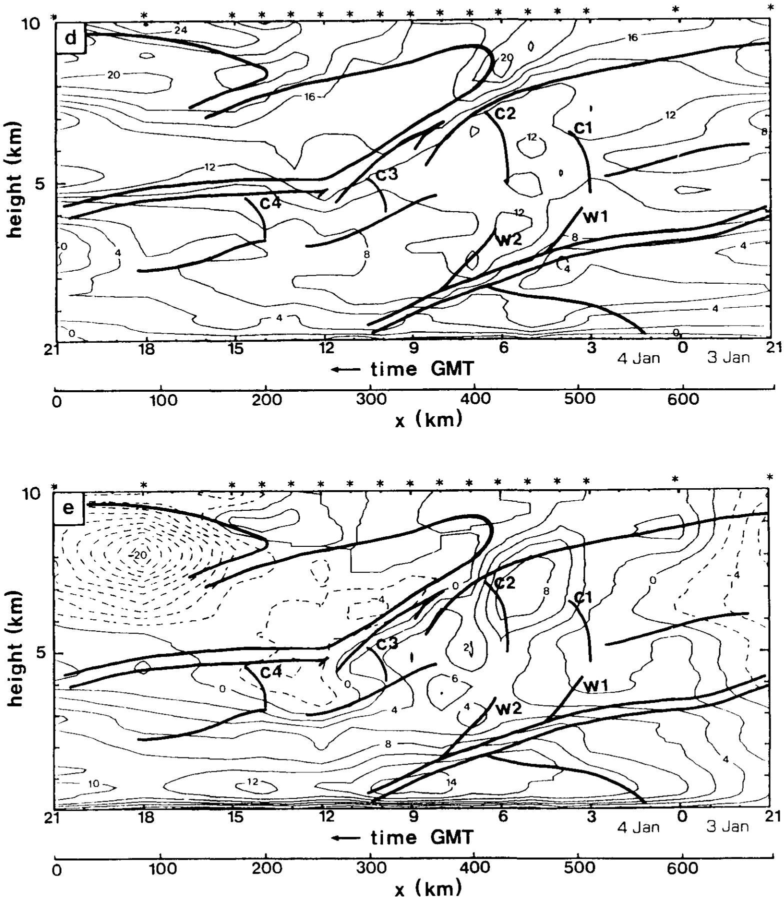

Wet-bulb potential temperature (°C). In this and the subsequent figures some of the baroclinic zones of Fig. 4a are also shown. (c) Relative humidity (%). Values >90% stippled. (d) West–east component of the wind (m/s). (d) South–north component of the wind (m/s).

account the northward ascent of the topography.

In the following time-height sections, the vertical and horizontal axes correspond to those represented in the previous cross-section from the Lammi sounding station. However, as Lammi was situated at the eastern side of the sounding triangle and the derivatives represent the mean values inside the triangle, the cross-sections for Lammi must be shifted about 1 h (30 km) to the right to correspond to the subsequent figures.

Fig. 5a shows the time–height section of the mean divergence over the sounding triangle. Zones of convergence are observed related to the warm frontal layers. There is also frictional convergence near the surface. In the lower half of the troposphere, the divergence shows values between $-5 \ldots +4 \times 10^{-5}\ s^{-1}$. At higher levels close to the tropopause, these limits are slightly exceeded. Comparing the pattern of divergence observed in this study to that deduced from Doppler radar observations by Heymsfield (1979) and Browning and Harrold (1969), a similar structure can be found. However, in their studies, the maximum and minimum values of divergence were almost an order of magnitude greater, which can be explained by the smaller observational area of the Doppler radar and also by the relative weakness of the front in our case.

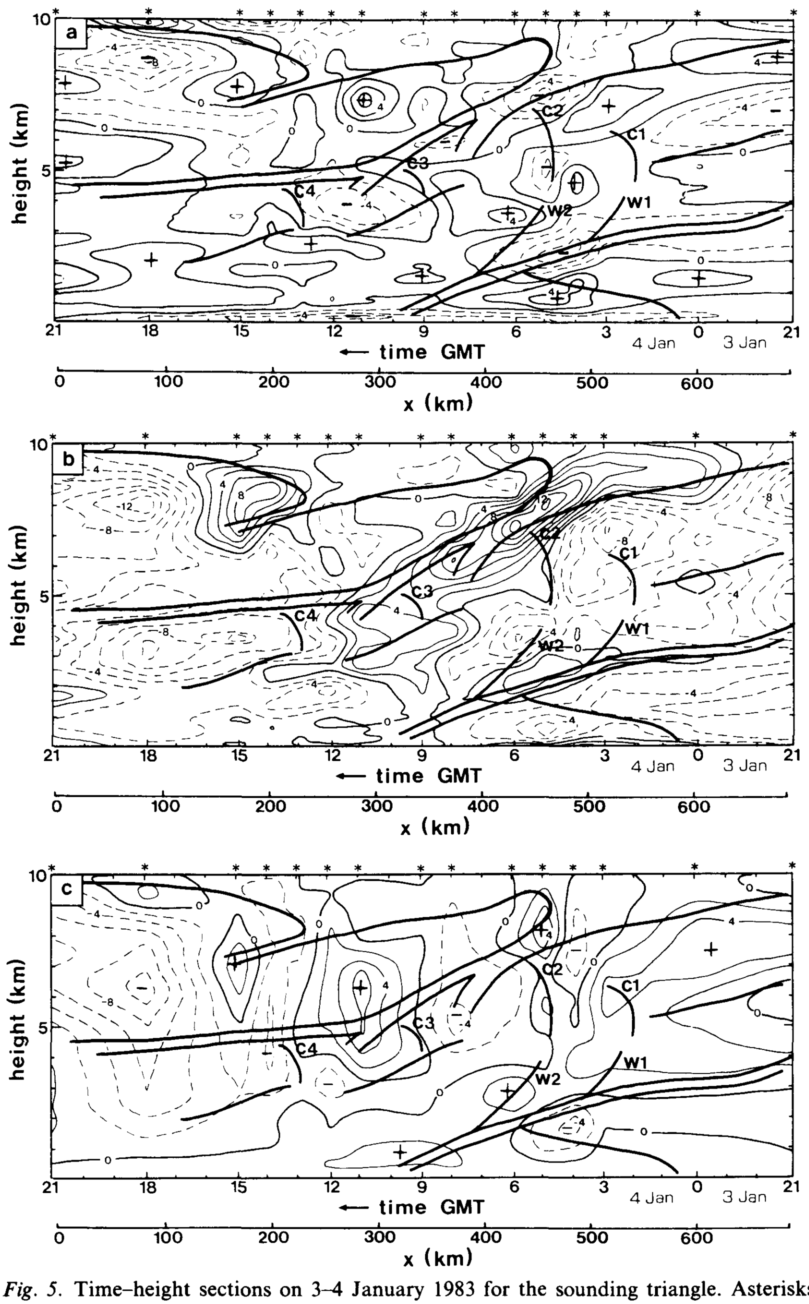

Fig. 5. Time–height sections on 3–4 January 1983 for the sounding triangle. Asterisks at the top of each figure indicate times of radiosonde soundings. (a) divergence ($10^{-5}\ s^{-1}$), (b) relative vorticity ($10^{-5}\ s^{-1}$), (c) vertical velocity (cm/s). In each figure, baroclinic zones as in Fig. 4b are shown.

The time–height section of the vertical component of relative vorticity is shown in Fig. 5b. Positive vorticity is observed along the warm frontal zones, the maximum values being at the upper warm frontal zone about $1.5 \times 10^{-4}\ s^{-1}$. Local maxima of positive vorticity can be found in relation to the major cold surges. This is a consequence of the typical distribution of the v-component of the wind in connection with the cold surges. Again, with the most baroclinic surges (C2 and C3), the values of vorticity are highest, while with the surges C1 and C4, the vorticity is closer to zero or even negative.

Fig. 5c is the time–height section of the vertical velocity. Considering the sensitivity of the method used to even small errors in the horizontal divergence, the observed pattern fits surprisingly well with the frontal structures. There is a more-or-less uniform layer of ascending motion of 1–2 cm/s above and within the lowest warm frontal zone continuing in the boundary layer behind the surface front. Descending motion can be observed beneath and ahead of the front and in the free atmosphere behind the surface front. Compared with the corresponding analysis of the relative humidity (Fig. 4c), the correlation is very good; moist regions behind the front are capped by subsidence. The dry air beneath the warm front is also related to descending motion.

Two main cores of ascending motion in the mid-troposphere with maximum values of 4 and 6 cm/s correlate surprisingly well with the cold surges. There is ascending motion in front of and descending motion behind surges C1, C2 and C4. Also, the humidity has local maxima related to the ascending parts of the cold surges. In the rear portions of the system, the air is generally descending with a maximum value of 10 cm/s.

4.3. Horizontal structure of the cold surges and warm tongues

The horizontal extent of the cold surges and warm tongues apparent from the time–height sections is too small to be discernible from the synoptic scale upper air analyses. From the sounding data of this experiment, pseudo-horizontal analyses (horizontal time-sections) can be derived using time series from the stations of Lammi and Vaisala which were situated almost parallel to the front at a distance of 90 km from each other.

Figs. 6a, b show the pseudo-horizontal fields of temperature at 450 and 700 hPa, respectively. The zones of sharp temperature gradient ahead of the cold surges and warm tongues can be seen. To help with identification, the cold surges and warm tongues seen in the vertical cross-sections and the location of the horizontal cross-sections are also shown. In connection with the cold surges, the maximum horizontal temperature gradient was 0.6 K/10 km, which is slightly greater than the values observed by Shakina et al. (1984) by aircraft in otherwise similar fronts. It is also worth emphasizing that the cold surges are N–S oriented.

Consistent with the field of vorticity, weak troughs related to the cold surges could be observed from the pseudo-horizontal cross-section of the geopotential (not shown here). Similar observations can be found in Elliott and Hovind (1965).

The orientation of the warm tongues (Fig. 6b) is similar to that of the warm frontal zone, i.e., NNW–SSE, while vertically they are forward and upward sloping. The maximum horizontal temperature gradient of the most prominent warm tongue was 0.5 K/10 km.

4.4. Composite frontal structures and precipitation patterns

Fig. 7 shows a composite representation of the frontal structures of this warm occlusion. Fig. 7a shows the horizontal winds relative to the movement of the lowest warm front superimposed on the frontal structures derived in Subsection 4.1. The estimated locations of the cold and cool conveyor belt flows are also indicated. Reflection of the baroclinic structures can be seen clearly in the front-relative winds. Across the cold surges, relative winds behave more-or-less like winds across ordinary fronts.

In Fig. 7b, the precipitation bands observed by weather radar are shown as contours of equivalent radar reflectivity factor. The values shown are basically averages over a small quasi-horizontal sector in the middle of the sounding triangle, representing triangle-mean reflectivities. Based on these values at different elevations, vertical distributions are derived from each three-dimensional measurement at 10 min intervals, and the resulting composite time–height section is superimposed on the frontal structures. Isolines of relative humidity of 50, 70 and 90% observed in Lammi are included.

The precipitation in this warm occluded front was arranged into 2 major precipitation bands (B1 and B2 in Fig. 7b) with a wavelength of

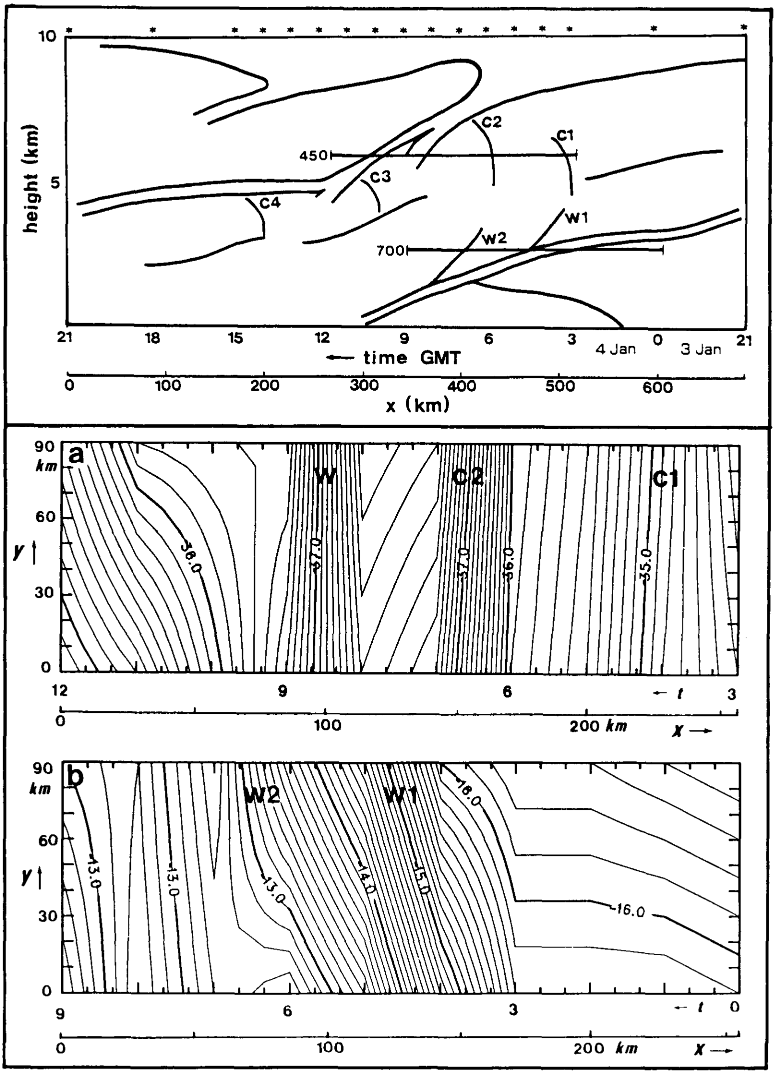

Fig. 6. Upper panel: Baroclinic zones as in Fig. 4b. Horizontal bars: locations of the horizontal time sections in (a) and (b). The heights of the time sections are shown in hPa. Lower panel: Horizontal time-section of the temperature (°C) derived from the time cross-sections of Lammi and Vaisåla (see Fig. 1) at the levels of (a) 450 hPa, (b) 700 hPa.

about 100 km. The last band was composed of 2 smaller bands with a wavelength of about 30 km. The precipitation from the 1st major band did not reach the ground due to the dry air-mass below. Though it is not obvious from the radar reflectivity cross-section, the satellite pictures (Fig. 2) show very clearly that the leading part of the frontal cloud also comprised a series of bands with a wavelength of about 100 km.

The radar echoes only reached a height of 3–4 km, which is typical of wintertime cases. However, according to aircraft reports, a cloud layer was observed ahead of the cold surge C2 at heights of between 4800–5400 m with snowfall

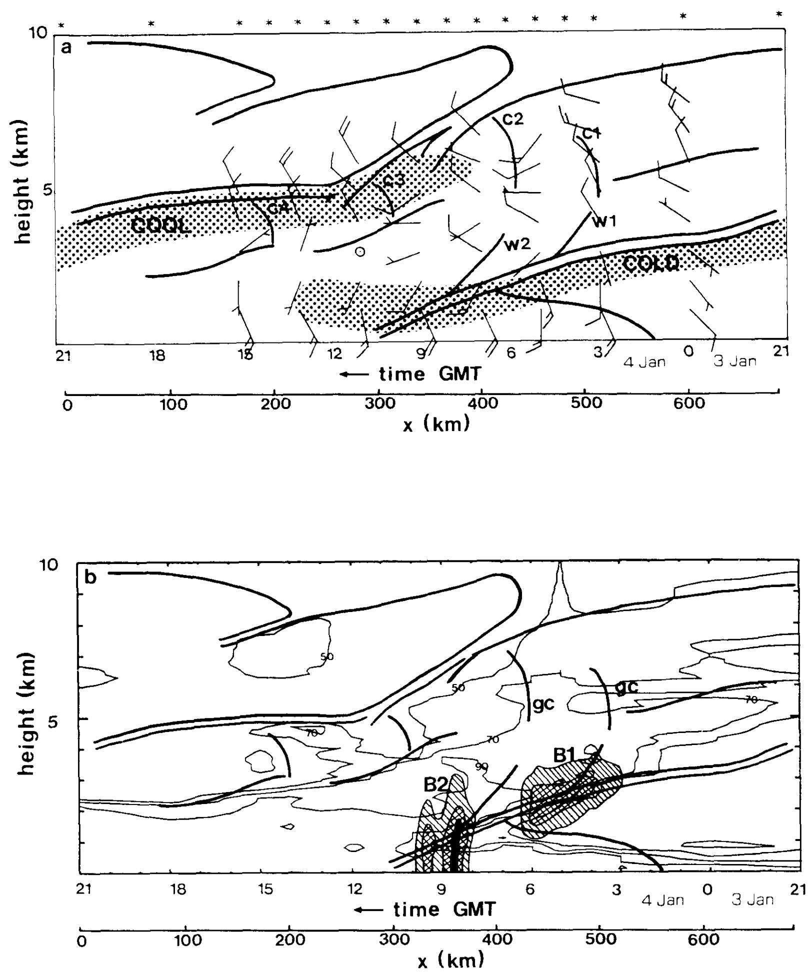

Fig. 7. A composite time-height section of some main features for the case 3–4 January 1983. (a) Horizontal winds relative to the movement of the lowest warm front. Short barb = 2.5 m/s, long barb = 5 m/s. Heavy line: baroclinic zones as in Fig. 4b. (b) Solid line: relative humidity (%). B1 and B2 denote the two major precipitation bands. Hatching: equivalent radar reflectivity factor Z_e, $5 < Z_e < 15$ dBZ_e, cross-hatching: $15 < Z_e < 20$ dBZ_e, shaded: $Z_e > 20$ dBZ_e. GC: The estimated location of the generating cells. Baroclinic zones as in (a).

below that layer. This is an indication of the existence of generating cells at heights from which no radar echoes were received. It is most probable, considering the small terminal velocity and large drifting distance of snow crystals, that the generating cells responsible for the enhanced snowfall in the bands B1 and B2 were situated just ahead of the cold surges C1 and C2, respectively, corresponding to the 2 main bands of high clouds seen in the satellite picture of Fig. 2c.

Severe icing was reported by aircraft pilots within the bands (especially within B2) and in the moist air between them. As a consequence, the snow crystals observed on the ground were in the form of heavily-rimed graupel. This suggests that the production of ice crystals in the generating cells was not sufficient to extract all the condensed cloud water in the lower parts of the frontal zone. This may partly be related to the fact that the updraughts were no longer vigorous enough to produce significant snowfall aloft in this decaying stage of the front. The absence of

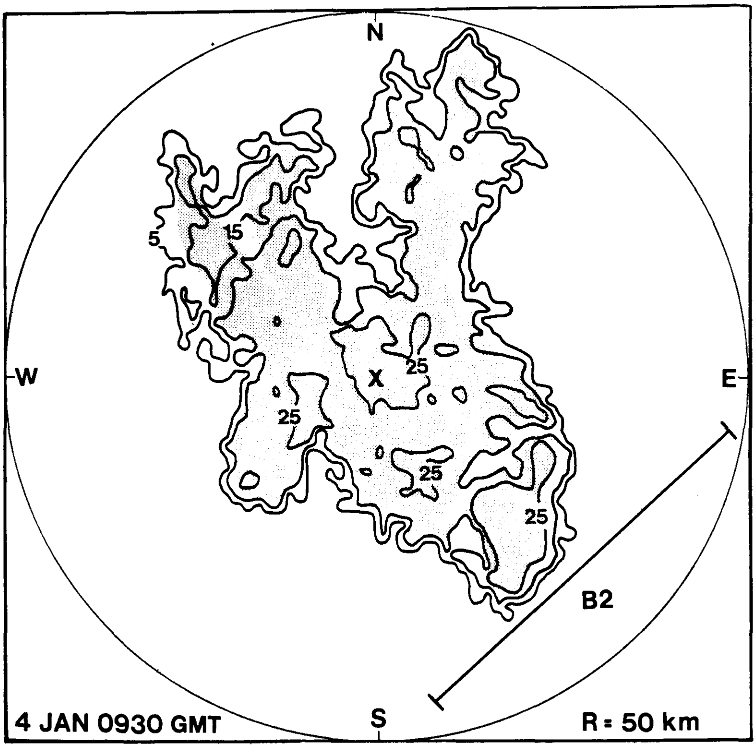

Fig. 8. The PPI-scan of radar reflectivity on 4 January 1983 at 0930 GMT at 1.5° elevation angle. The radius of the scan is 50 km. The cross denotes the position of the radar. B2 as in Fig. 7b.

the upper-level "seeder" cloud was very evident in the post-frontal parts of the system, where only slight drizzle was produced from the 3 km deep moist layer capped by relativley dry and subsiding air. The mean total precipitation amount from this front over our study area was only 0.5 mm.

A low-elevation angle PPI-scan of radar reflectivity on 4 January 1983 at 0930 GMT is shown in Fig. 8. The lowest reflectivity value shown is 5 dB above the noise level. The echoes seen in this figure correspond to the 2 bands 30 km apart inside the band B2 in the previous figure. Although there are 2 distinct NNW–SSE-oriented banded patterns of maximum reflectivity, one can also see there some indications of patterns that are rather N–S-oriented. Comparing this observation to the orientation of the hyperbaroclinic zones in Fig. 6, one can conclude that the N–S structures may be connected with the generating cells ahead of the cold surges, whereas the NNW–SSE bands are most probably related to the warm tongues over the lowest warm frontal zone. The NNW–SSE bands moved with the velocity of the warm frontal zone, i.e., 8 m/s to the ENE.

This feature of rainbands crossing each other seems to be a rule rather than an exception in occlusions, and has already been noted by Saarikivi (1983). It is worth emphasizing that the bands with different orientations often maintain their characteristics even though they cross each other.

Besides the two main frontal precipitation bands, shorter-wavelength bands approximately parallel with the mean boundary layer wind can possibly be detected from the radar data. They look very much like the horizontal roll vortices found by Puhakka and Saarikivi (1986) in many frontal cases. Due to the lack of detailed infor-

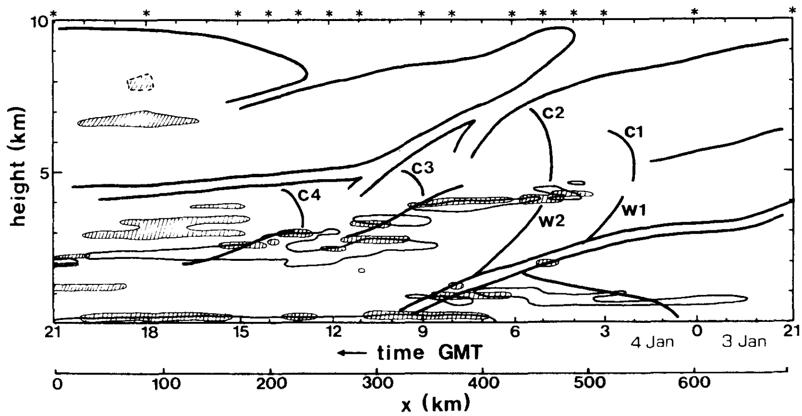

Fig. 9. Time–height section of some instability parameters on 3–4 January 1983. Continuous line: potentially unstable areas. Hatching: areas with CSI. Dashed line: inertially unstable area. Heavy lines: baroclinic zones as in Fig. 4b.

mation on the flow pattern from a Doppler radar, possible roll circulations could not be directly detected.

5. Instability mechanisms

The main reason for the precipitation in this case was the frontal lifting of the moist southwesterly flow. The 2 major precipitation bands were clearly related to the warm tongues and cold surges of air above the warm frontal zone. The precipitation bands may have formed due to the release of potential instabilty in connection with the frontal lifting. The whole upper portion of the moist flow was potentially unstable, as can be seen from Fig. 9, which shows a time–height section of some instability parameters over the areas of the sounding triangle. The areas of negative vertical gradient of moist potential temperature, indicating potentially unstable areas, are enclosed with full lines. The whole frontal region was hydrostatically stable or moist neutral and only locally slightly conditionally unstable in some shallow layers.

One question to be answered is the reason for the occurrence of the warm tongues and cold pulses and the related precipitation bands about 100 km from each other. This wavelength is typically mesoscale, and there are not many possible instability mechanisms that produce perturbations on that scale in the atmosphere. One explanation for patterns of this wavelength may be conditional symmetric instability, CSI, first proposed by Bennetts and Hoskins (1979) as a possible explanation for frontal rainbands. The growth rate parameter σ^2 of CSI was evaluated following Bennetts and Sharp (1982) using the formula

$$\sigma^2 \approx -f\eta + f\left(\boldsymbol{k} \times \frac{\partial \boldsymbol{V}_{\rm h}}{\partial z} \cdot \nabla_{\rm h}\,\theta_{\rm w}\right)\Big/(\partial\theta_{\rm w}/\partial z),$$

where f is the Coriolis parameter, η is the vertical component of the absolute vorticity vector, $\boldsymbol{k}$ is the unit vector along the vertical axis, $\boldsymbol{V}$ is the wind vector, and subscript h refers to a horizontal vector or operator.

Positive values of the growth rate of CSI are shown by hatching in Fig. 9. It can be seen that there were just a few minor areas in the vicinity of the rainbands which were slightly conditionally symmetrically unstable, and most of those areas were due to a zero or negative vertical gradient of wet-bulb potential temperature. However, in the rear part of the frontal system, positive growth rates of pure CSI were observed within 2 layers at 2.5–4 and 6.5–7 km. 2 very small spots of pure CSI were also apparent in the warm frontal zone under the warm tongues.

Based on values of the growth rate parameter alone, one cannot conclude that the observed mesoscale circulations above the warm occluded frontal zone were caused by CSI, since by this stage the atmosphere had already adjusted and became neutral to any possible moist symmetric instability which may have existed earlier over the forward part of the frontal zone. Thus, the growth rate parameter no longer shows positive values there, except very locally. The positive values of CSI growth rate in the post-frontal parts of the system may indicate that CSI is inducing symmetric circulations there which gradually, after drifting over the frontal zone, render the atmosphere neutral to CSI.

The obvious resemblance of the observed structures of humidity, horizontal wind, vertical velocity and temperature in connection with the cold surges and warm tongues, to the corresponding structures from the numerical experiments with CSI by Saitoh and Tanaka (1987), gives rise to the deduction that similar physical mechanisms should be responsible in both cases. In our observations, there are distinct thermally-direct slantwise rolls parallel with the mean geostrophic shear connected with the cold surges and warm tongues over the main baroclinic zone. The wavelength of the perturbations, about 100 km, is in accordance with the theory and can be obtained from the depth of the unstable layer (1.5 km) and the slope of the θ_w surfaces in that layer as estimated by Selzer et al. (1985). The smaller 30-km wavelength between the minor bands inside the main warm frontal snow band also fits exactly the wavelength induced due to release of potential instability according to the model of Saitoh and Tanaka. The updraughts ahead of the cold surges are relatively moist and the downdraughts behind are dry, which is a natural consequence in these thermally-direct circulations.

The observed field of the front-parallel wind component is important when considering the transport of heat in cyclones. As shown by Saitoh and Tanaka (1987), the main task of symmetric perturbations in cyclones is to assist in the poleward flux of heat. In our case, this tendency is very pronounced in the flow patterns connected with cold surges C2 and C3. In surges C1 and C4, this characteristic is not observed, probably indicating that the first roll had already decayed, while the last one had not yet generated the baroclinicity required for the typical distribution of the v-component. This is consistent with the aforementioned indications of roll development and occurrence of CSI in various parts of the frontal system.

One question to be answered is that concerning the mechanism maintaining CSI in this old decaying front. Obviously the reason for the favourable conditions for CSI above the moist occluded warm frontal zone is the differential temperature advection caused by the relatively cool and dry airflow descending from the mid-troposphere above the frontal zone. Differential temperature advection was also responsible for the occurrence of CSI in the case studied by Wolfsberg et al. (1986).

Satellite observations from 3 January 00 GMT onwards (not shown) indicate, that the bandedness in the frontal clouds was greatly enhanced after the front passed the Norwegian mountains. This may have been an additional mechanism triggering slantwise convection inside and above the moist layer above the frontal zone. The satellite pictures also show that the cloud bands continuously evolved and changed their form, indicating that the life-time of a single band may have been as short as, say, a few hours. Wolfsberg et al. (1986) report bands existing as individual entities for less than 4 h, but in our case, it is very likely that the 2 major bands observed by the weather radar and radio-soundings had longer life-times than that.

6. Conclusions

A case study of a winter-time deeply occluded cyclone using serial radiosonde soundings, weather radar and aircraft data revealed complex subsynoptic structures inside the synoptic-scale frontal zone observable by conventional methods. The observations seemed to lend substance to the aforementioned assertion by Wallace and Hobbs (1977), as this elongated (about 2000 km long) occlusion principally had the structure of a warm front. The zone of cold advection above the main warm moist flow was, however, very typical of an occlusion.

Compared to previous studies of somewhat similar fronts by Elliott and Hovind (1965), Browning et al. (1973) and Heymsfield (1979), our case differed in some respects. Firstly, in our case, no melting layer was present, as the temperature was in general below zero everywhere in the troposphere during the frontal passage. Thus, the bright band effect was insignificant in the radar measurements, and melting could not produce any additional effects on the frontal dynamics. Secondly, the main front was capped by another front connected to the next member of the cyclone family, continuously closing in on the leading one. Thirdly, our front was in a decaying stage and occurred in a general large-scale flow of strong diffluence. Thus, it was surprising that the structures observed were still very pronounced.

It was also shown that using the concepts of warm and cold conveyor belt flows as proposed by Harrold (1973) and Browning et al. (1973), all stages of the development could not be explained. In this particular case, another cool mid-tropospheric airflow had to be considered in addition to the WCB and CCB. As that flow descended from about 500 hPa behind the fronts to cap the warm moist air just above the occluded and warm fronts, it resembled the mid-tropospheric flow of potentially cold air, leading to instability above the WCB, described by Harrold (1973) and Browning et al. (1973). Also different in this case was the presence of two main branches in the mid-tropospheric air: one turning anticyclonically above the occlusion point as in the model of Harrold and Browning, the other turning cyclonically towards the cyclone centre. This structure above the moist, relatively warm air of the occluded front maintains potential instability near the cyclone centre, but in those areas where the relatively cool air descends to, or sinks below the height of the remains of the WCB close to the occlusion point, the frontal system stabilizes and may finally lose its original connection with the mother cyclone.

The complex thermodynamical structure common to previous observations of occlusions was also found in this case study. Surges of cold air above the warm and moist layer of air, and warm tongues within the moist layer were observed. These were connected with the 2 major precipitation bands of the system.

The observed banded thermodynamical and kinematic structures, which basically were overlapping zones of slantwise thermally-direct circulations, were similar to those caused by conditional symmetric instability, which in this case was postulated to be the most probable cause for these structures.

It was not possible, based on the data of this study, to show definitely what kind of circulations were related to the cold surges and warm tongues. Whether they develop in pairs having a common thermally-direct circulation, or whether there are two independent sets of circulations remains to be answered. Other problems for future studies are the relative movement and interactions between cold surges and warm tongues, the life cycle of these circulations and their possible drifting across the frontal zones.

However, it has been shown that the circulations related to warm tongues and cold surges together transfer warm air upwards and northwards; the warm tongues supply warm and moist air up at the top of the moist layer above the warm frontal surface, where the cold surges raise the same air higher still. Between the air supplied by the warm tongues and the cooler air from cold surges, cold-front-like baroclinic zones form. Related to these baroclinic zones, a systematic difference across the zone in the zone-parallel wind component forms causing a net effect of poleward temperature flux.

This study and other recent experimental studies indicate that the classical Norwegian occlusion model is far too simplified to give the typical characteristic features of the occlusion process in extratropical cyclones. Much more observational work needs to be done with the finest possible resolution in time and space to reveal the small-scale features of both warm and cold-type occlusions in the various life stages of cyclones.

7. Acknowledgements

Financial support for this study was received from the Academy of Finland, the Vaisala Company, the Aili Nurminen, the Sohlberg, the Heikki and Hilma Honkanen, and the Vilho, Yrjö and Kalle Väisälä Foundations.

REFERENCES

Bennetts, D. A. and Hoskins, B. J. 1979. Conditional symmetric instability—a possible explanation for frontal rainbands. *Quart. J. R. Met. Soc. 105*, 945–962.

Bennetts, D. A. and Sharp, J. C. 1982. The relevance of conditional symmetric instability to the prediction of mesoscale frontal rainbands. *Quart. J. R. Met. Soc. 108*, 595–602.

Bergeron, T. 1937. On the physics of fronts. *Bull. Amer. Met. Soc. 18*, 265–275.

Bergeron, T. 1959. Methods in scientific weather analysis and forecasting. An outline in the history of ideas and hints at a program. In: *The atmosphere and the sea in motion* (ed. B. Bolin). New York: Rockefeller Inst. Press, 440–474.

Browning, K. A. and Harrold, T. W. 1969. Air motion and precipitation growth in a wave depression. *Quart. J. R. Met. Soc. 95*, 288–309.

Browning, K. A., Hardman, M. E., Harrold, T. W. and Pardoe, C. W. 1973. The structure of rainbands within a midlatitude depression. *Quart. J. R. Met. Soc. 99*, 215–231.

Carlson, T. N. 1980. Airflow through midlatitude cyclones and the comma cloud pattern. *Mon. Wea. Rev. 108*, 1498–1509.

Elliott, R. D. and Hovind, E. L. 1965. Heat, water and vorticity balance in frontal zones. *J. Appl. Meteor. 4*, 196–211.

Godson, W. L. 1951. The synoptic properties of frontal surfaces. *Quart. J. Roy. Met. Soc. 77*, 633–653.

Harrold, T. W. 1973. Mechanisms influencing the distribution of precipitation within baroclinic disturbances. *Quart. J. Roy. Met. Soc. 99*, 232–251.

Herzegh, P. H. and Hobbs, P. V. 1981. The mesoscale and microscale structure and organization of clouds and precipitation in midlatitude cyclones. IV: Vertical air motions and microphysical structures of prefrontal surge clouds and cold-frontal clouds. *J. Atmos. Sci. 38*, 1771–1784.

Heymsfield, G. M. 1979. Doppler radar study of a warm frontal region. *J. Atmos. Sci. 36*, 2093–2107.

Hobbs, P. V., Houze, R. A., Jr. and Matejka, T. J. 1975. The dynamical and microphysical structure of an occluded frontal system and its modification by orography. *J. Atmos. Sci. 32*, 1542–1562.

Houze, R. A., Jr., Locatelli, J. D. and Hobbs, P. V. 1976. Dynamics and cloud microphysics of the rainbands in an occluded frontal system. *J. Atmos. Sci. 33*, 1921–1936.

Kreitzberg, C. W. 1964. The structure of occlusions as determined from serial ascents and vertically-directed radar. Air Force Cambridge Research Lab. *Rept. AFCRL-64-26*, 121 pp.

Kreitzberg, C. W. 1968. The mesoscale wind field in an occlusion. *J. Appl. Meteor. 7*, 53–67.

Kreitzberg, C. W. and Brown, H. A. 1970. Mesoscale weather systems within an occlusion. *J. Appl. Meteor. 9*, 417–432.

Kurz, M. 1988. Development of cloud distribution and relative motions during the mature and occlusion stage of a typical cyclone development. Preprints, *Palmén Memorial Symposium on Extratropical cyclones*, Helsinki, Finland 29 August–2 September, 1988. Boston: Amer. Met. Soc., 201–204.

Matkovskii, B. M. and Shakina, N. P. 1982. Mesoscale structure of an occluded front over the center of the European USSR from special measurements. *Meteorologiya i Gidrologiya*, No. 1, 24–33.

Nash, J. and Schmidlin, F. J. 1987. WMO international radiosonde comparison (U.K. 1984, U.S.A. 1985), Final report. Instruments and observing methods, *Report No. 30. WMO/TD-no. 195*, 103 pp.

Palmén, E. 1951. The aerology of extratropical disturbances. In: *Compendium of Meteorology*. Boston: Amer. Met. Soc., 599–620.

Puhakka, T. and Saarikivi, P. 1986. Doppler radar observations of roll vortices in Finland. *Geophysica 22*, Nos. 1–2, 101–118.

Ragette, G. 1984. Analysis of a frontal system over central Europe. *Beitr. Phys. Atmosph. 57*, 447–462.

Saarikivi, P. 1983. Radar observations of snowbands in Finland—a preliminary report. In: *Mesoscale meteorology—theories, observations and models* (eds. D. K. Lilly and T. Gal-Chen). Dordrecht/Holland: D. Reidel Publ. Comp., 285–292.

Saarikivi, P. and Puhakka, T. 1986. Mesoscale rain and snowfall experiment: objectives and observational procedures. Department of Meteorology, Univ. of Helsinki, *Report No. 27*, 36 pp.

Saitoh, S. and Tanaka, H. 1987. Numerical experiments of conditional symmetric baroclinic instability as a possible cause for frontal rainband formation. Part I. A basic experiment. *J. Met. Soc. Japan 65*, 675–708.

Selzer, M. A., Passarelli, R. E. and Emanuel, K. A. 1985. The possible role of symmetric instability in the formation of precipitation bands. *J. Atmos. Sci. 42*, 2207–2219.

Shakina, N. P., Postnov, A. A. and Lyakhov, A. A. 1984. Layered sloping mesoscale structures and rainbands in atmospheric frontal regions and their relation to symmetric instability. *Proc. Nowcasting-II Symposium*, Norrköping, Sweden, 3–7 Sept., 1984. ESA SP-208, 57–62.

Vuorela, L. 1953. On the air flow connected with the invasion of upper tropical air over northwestern Europe. *Geophysica 4*, 105–130.

Wallace, J. M. and Hobbs, P. V. 1977. *Atmospheric Science: An introductory survey*. New York: Academic Press, 467 pp.

Wolfsberg, D. G., Emanuel, K. A. and Passarelli, R. E. 1986. Band formation in a New England winter storm. *Mon. Wea. Rev. 114*, 1552–1569.